

# Exploration of the Survival Probability and Shape Evolution of Crushable Particles During One-dimensional Compression Using Dyed Gypsum Particles

Jidu Yu<sup>1</sup>, Graduate Research Assistant; Chaomin Shen<sup>2\*</sup>, Ph.D.; Sihong Liu<sup>3</sup>, Ph.D., Professor;

Yi Pik Cheng<sup>4</sup>, Ph.D., Associate Professor

**Abstract:** Observing the fragmentation of individual particles within granular assemblies is a subject of evident theoretical and practical importance. A new technique using dyed gypsum particles (DGPs) to match the broken particles to their parents was adopted in this study. An image-based method of acquiring the shape information of particles from two orthogonal views was proposed. The mass survival probability and shape characteristics of the children particles were analyzed after a series of one-dimensional compression tests on the DGPs. It was found that medium-sized particles in the polydisperse samples underwent more breakage than the other particles, and this might have been attributed to the combined effects of the particle crushing strength and the coordination number. The shape evolution of broken particles and surviving particles showed opposite trends. As the particles after the test within a given size range consisted of both the broken and surviving particles, their overall shape characteristics did not show a consistent trend. Furthermore, individual particle crushing tests on the children particles suggested that the breakage-induced shape irregularity did not change the Weibull modulus, but had a substantial effect on the magnitude of the survival probability.

**Keywords:** Dyed gypsum particle; Particle crushing; Particle shape; Survival probability; Oedometer test

- 
1. Graduate Research Assistant, College of Water Conservancy and Hydropower Engineering, Hohai University, Nanjing 210098, China. Email: yujidu126@gmail.com
  2. Postdoctoral Research Fellow, College of Water Conservancy and Hydropower Engineering, Hohai University, Nanjing 210098, China. Email: chaomin.shen@hotmail.fr
  3. Professor, College of Water Conservancy and Hydropower Engineering, Hohai University, Nanjing 210098, China. Email: sihongliu@hhu.edu.cn
  4. Associate Professor, Department of Civil, Environmental and Geomatic Engineering, University College London, London WC1E 6BT, United Kingdom. Email: yi.cheng@ucl.ac.uk

\* **Corresponding author:** Chaomin Shen. Email: chaomin.shen@hotmail.fr

## Introduction

Particle crushing occurs commonly in geotechnical engineering processes, e.g., the construction of high rockfill dams (Tapias et al. 2015; Jia et al. 2017; Xiao et al. 2018), the cyclic loading of railway ballast (Lu and McDowell 2010; Indraratna et al. 2015; Sun et al. 2016), and the installation of piles penetrating into crushable soils (Jardine et al. 2013; Mao et al. 2019). The crushability of particles is related to many factors such as the particle size, particle size distribution (PSD), particle shape, lithology, density, and stress level (McDowell and Bolton 1998; Nakata et al. 1999; Alonso et al. 2012; Xiao et al. 2018). Particle crushing leads to changes in the particle size and shape, and further influences the compressibility, shear strength, seepage, and time-dependent behavior of particle aggregates (Cheng et al. 2004; Kwok and Bolton 2013; Xiao et al. 2016; Jia et al. 2017; Liu et al. 2018). More recently, the evolution of the particle size and shape during particle crushing has drawn attention in the numerical simulation and constitutive modeling of crushable granular soils.

The survival probability is a statistical quantity for particle crushing. Extensive experimental results on the crushing of single particles show that the survival probability of a single particle decreases with increasing particle size and satisfies the Weibull distribution (McDowell and Bolton 1998; Nakata et al. 1999; Cheng et al. 2003). Despite the efforts to use statistics to describe the amount of grain crushing at the particulate level, the relative breakage indexes based on an overall change in the PSD (e.g., Marsal 1967; Hardin 1985; Lade et al. 1996; Einav 2007; Wood and Maeda 2008) are still commonly used to quantify the degree of crushing in engineering practice. This is because it is hard to perform experiments to investigate the survival probability of particles in assemblies, due to the difficulty in determining whether one particle suffers from crushing in an assembly. The survival probability of particles in assemblies is influenced by not only the particle size but also other complex factors, such as the coordination number and the contact force. These interparticle variables are not easy to quantify in conventional geotechnical experiments. Wiebicke et al. (2017) and Hurley et al. (2016) recently reported the application of X-ray tomography images in detecting interparticle contacts and forces, which could be extended to the particle crushing process. Even so, there is

still a lack of knowledge to be able to establish the quantitative connection between the macroscopic and particulate scales. It would be of great interest to break through the conventional experimental techniques to observe the fragmentation of individual particles in assemblies. More recently, Peng et al. (2019) carried out one-dimensional (1D) compression tests on dyed coral sands and quantified particle crushing using the "absolute particle breakage" index by excluding the amount that migrated from larger particles. This newly defined breakage index is, by definition, the survival probability of particles within a size range.

The particle shapes are usually characterized by several shape factors, such as the convexity, sphericity and aspect ratio (Barrett 1980; Cho et al. 2006; Altuhafi et al. 2013). In 1D compression tests, well-graded particles obtain a small amount of abrasion along with a reduction in surface roughness, whereas uniform particles suffer from catastrophic splitting, generating children particles whose shapes are more irregular than their parents (Altuhafi and Coop 2016). The shape evolution of uniform particles in ring shear tests is quite different, where particles tend to become smoother and more rounded after the test (Zhang et al. 2018). If samples are repeatedly reconstituted and reloaded, particle shapes will continuously change and finally reach a stable state where the evolution of the PSDs also stops (Yan and Shi 2014). Generally, these results are analyzed based on the average shape factors of overall particles within a size range. However, the average value ignores many details, such as the difference between the surviving particles and broken particles and the statistical distribution of the shape factors. In addition, as an increasing number of studies on particle crushing focus on simulating more realistic-shaped particles (Ferrellec and McDowell 2010; Eliáš 2014; Gladky and Kuna 2017), more detailed experimental data are needed for the calibration and comparison of such studies.

In this study, the survival probabilities of particles under 1D compression were explored by using dyed gypsum particles (DGPs), which allowed the broken fragments to be easily matched to the parent particles according to their color. Detailed investigations on the evolution of the particle breakage and the particle shape factors were performed. The influence of the breakage-induced shape irregularity on the particle crushing statistics was further investigated.

## Preparation of the Dyed Gypsum Particles

Dyeing is an effective way to track research targets and has been widely used in biological science. Nakata et al. (2001) pioneered the use of this method for geotechnical granular materials, where dyed silica sands were seeded in specimens to observe the fracture characteristics of individual particles during 1D compression. Subsequently, although this method has been adopted in some studies (e.g. Wang et al. 2017; Peng et al. 2019), it is not common since it is difficult for the color to penetrate into the interior of natural particles, especially larger particles. To ensure that the color of the particles is uniform, dyed gypsum particles (DGPs) produced from the gypsum powder and dyed water were used as the testing materials in this study instead of dyed natural granules.

As a cementing material, gypsum is widely used in various tests and is also a popular raw material for the 3D printing of geotechnical materials (Kong et al. 2018a, 2018b; Kittu et al. 2019; Wu 2019). The gypsum powder used in this study, which is high-strength  $\alpha$ -hemihydrate gypsum ( $\text{CaSO}_4 \cdot 1/2\text{H}_2\text{O}$ ), was produced by the Shanghai Huaqiang Gypsum Factory. Table 1 shows the properties of the gypsum. The gypsum boards (Fig. 1(a)) with a size of 280 mm  $\times$  220 mm  $\times$  80 mm were manufactured from this powder. The manufacturing process of the gypsum boards was similar to that of concrete. During the process, bubbles in the gypsum paste were discharged by vibration to reduce defects in the particles. DGPs were mechanically crushed from the gypsum boards by a hammer with varying amounts of inputting work, so that the majority of the particle sizes were roughly located in the desired size range depending on their colors. Then, particles of undesired sizes were abandoned by sieving. It is worth mentioning that by adopting this preparation procedure, the initial shape of the particles does not substantially change with the particle size/color.

Fig.1(b) shows the artificial DGPs and their sizes. There are five groups of particles with different colors and size ranges, that is, grey particles (20.0-12.6 mm), green particles (12.6-7.9 mm), red particles (7.9-5.0 mm), yellow particles (5.0-3.1 mm), and blue particles (3.1-2.0 mm). The value of  $d_{50}$  for the DGPs of each color is a geometric sequence with a common ratio of  $\sqrt[3]{4}$ .

## Calculations of the Shape Factors

With the development of image acquisition and processing technology, it is convenient to obtain particle shape information by scanning or photographing. High resolution digital cameras with can be used to easily acquire particle images. Although it is possible to reconstruct 3D shapes by laser scanning technology (LST) or computed tomography (CT) (Yang et al. 2019), 2D methods are still irreplaceable in engineering and fundamental research due to their convenience, flexibility, and low cost. In this paper, both the top and side projections of the DGPs were photographed by cameras ( $4032 \times 3024$  pixels) so that some 3D shape characteristics could be analyzed. Fig. 2 illustrates the schematic diagram of the particle shape measurement. The base plate and the background plate are two blackboards that have a strong color contrast with the DGPs. Generally, when the particle is statically at rest, its orientation is not random but is in a stable state where the short-axis is vertical (Abbireddy and Clayton 2009). Two calibration scales were set up in two orthometric directions to measure the physical dimensions of the top and side projections. When photographed in the side direction, the particles were adjusted along a straight line with calibration scale 2, and the side camera was fixed in an appropriate position to prevent image distortion.

Many tools can be used to process images, such as ImageJ software (Prudêncio et al. 2013) and Imago Image Analysis System (Obaidat et al. 2017). In this study, a self-written MATLAB program was used, the results of which were confirmed to be correct by a comparison with the results obtained using ImageJ. Some basic parameters, such as the area ( $A$ ), the perimeter ( $P$ ), the diameter of an equivalent area circle ( $d_{EAC}$ ), the long size and short size Feret diameter ( $d_{L(top)}^F, d_{S(top)}^F$ ) from the top projection, and the height (short size) of the side projection ( $d_{S(side)}^F$ ), were measured so that four shape factors, i.e., the convexity ( $Cx$ ), the sphericity ( $S$ ), the aspect ratio ( $AR$ ), and the flatness ( $Fn$ ), could be calculated. Note that the Feret diameter was defined as the distance between two parallel lines tangent to the particle projection (Walton, 1948). The definitions of these shape factors are illustrated in Fig. 3 (Barrett 1980; Cho et al. 2006; Altuhafi et al. 2013). Note that  $Cx$ ,  $S$  and  $AR$  were measured from the top projection. The side projection was mainly measured for the

calculation of  $F_n$ . The flatness of the particles showed significant changes after 1D compression, which will be discussed later.

The digital image processing method can be applied not only to the measurement of the particle shapes but also to the analysis of the particle sizes. In this case, a polydisperse DGP sample ( $C_u=2.4$ ) was tested. Fig. 4 shows different PSDs using the sieve size,  $d_{L(top)}^F$ ,  $d_{S(top)}^F$ ,  $d_{avg(top)}^F$  and  $d_{EAC}$ . The PSD using  $d_{S(top)}^F$  nearly coincides with the PSD obtained by sieve analysis, while the other three PSDs are located to the right of the PSD obtained by the sieve analysis but with the same slope. Altuhafi et al. (2013) also performed the same comparison using QICPIC. In their study, the PSD using  $d_s^F$  was quite different from the PSD using sieve size. This is probably because the particles measured by QICPIC were randomly oriented, but in this study, the particles were placed at their lowest situation, as previously mentioned.

### Shape Characteristics of Parent DGPs

Table 2 shows the mean value of the shape factors of the parent DGPs. The mean values of  $Cx$ ,  $AR$ , and  $F_n$  for different-color groups are very similar with a difference of no more than 2.4%, while that of  $S$  is slightly higher with a difference of 3.3%. It is worth noting that the definition of  $S$  involves the particle perimeter, which is greatly affected by the image resolution, as was discussed by Mandelbrot (1983). Thus, errors are inevitable in the measurement of  $S$ , especially for the smaller particles with fewer pixels. However, the calculations of  $AR$  and the  $F_n$  are seldom affected by the image resolution.

The mean value of a shape factor is a basic indicator that reflects the average level of the particle shape, but the statistical distribution of the shape factor can be described by using the Weibull distribution function (Weibull et al. 1951):

$$F(x) = 1 - \exp \left[ - \left( \frac{x}{x_0} \right)^k \right] \quad (1)$$

where  $x$  is the value of the shape factor;  $x_0$  is the characteristic value of the shape factor;  $k$  is the Weibull modulus, which increases with decreasing distribution range; and  $F(x)$  is the cumulative frequency of the

shape factor. Fig. 5 shows the cumulative frequency  $F$  of the parent particles Grey<sub>BT-15.9</sub> and their fitted curves using Eq. (1). More fitting results for the other parent particles are listed in Table 3. The correlation coefficients ( $R^2$ ) are no less than 0.997 for all the cases. This proves that the Weibull distribution function is effective in describing the distribution of the shape factors.

## 1D Compression Test Program

Seven 1D compression tests were carried out on the DGPs, as shown in Table 4. test M1 was the main test, where more particle breakage and particle shape analysis were performed. tests U1- U5 and M2 were performed for comparison. The specimen of test M1 was a mixture of Grey<sub>BT-15.9</sub>, Green<sub>BT-10.0</sub>, Red<sub>BT-6.3</sub> and Yellow<sub>BT-4.0</sub> with a mass ratio of 1:1:1:1, so that the only variable in this test was the particle size. The specimens of tests U1- U5 were uniformly graded particles designed to compare the survival probability of the particles between test M1 and tests U1-U5. The specimen of test M2 consisted of blue<sub>BT-2.5</sub> and therefore had a larger initial size range compared to that of test M1.

The inner diameter of the oedometer cell used in these tests was 100 mm. Each sample weighed 600 g and was compacted to the densest state. The specific gravity  $G_s$  of the DGPs was measured at 2.30 according to the Chinese Code for the Specification of Soil test (SL237-1999). The initial void ratio was then calculated and is listed in Table 4. Theoretically, if particles, such as U1-U5, had parallel grading curves and similar particle shape, their packing densities should have been approximately the same, independent of their representative particle sizes. However, it can be seen from the test results that samples with larger particle sizes show relatively lower densities. This is mainly attributed to the wall/boundary effect (Jia and Williams 2001; Suzukia et al. 2008; Wang et al. 2018), i.e., there is a larger boundary zone for the samples with larger particles.

The walls of the oedometer cell were coated with Vaseline to reduce friction. All the samples were compressed to 6.4 MPa with a loading rate of 0.5 mm/min. Data on the vertical stress and displacement in the loading and unloading processes were collected once per second. Fig. 6 shows the compression curves

on  $e - \log \sigma_v$  plot. The compression curves of DGPs samples show obvious bilinearity, with the inflection point marked as the yield point of the material. The compressibility index  $C_c$ , which is equal to the gradient of the normal compression line (NCL), was calculated and is listed in Table 4. It can be seen that the uniformly graded samples with smaller particles have higher yield stresses but show no substantial difference in compressibility compared to those of the larger particles. This agrees with the experimental work by McDowell (2002), who further related the yield stress to the single-particle crushing strength. In addition, well-graded samples (M1 and M2) have higher packing densities, and the particles in these samples are protected by more surrounding particles; thus, well-graded samples have even higher yield stresses and lower compressibility than the uniformly graded samples.

### **Analyses of Particle Crushing during 1D Compression Tests**

After the 1D compression tests, particles were sieved and then separated according to their colors. Particles smaller than 2.0 mm in size were too small to analyze. Fig. 7 shows the after-test (AT) particles of test M1. Note that there are some particles still in their original size range, which are framed by the dotted lines in Fig. 7. These particles are called surviving particles, although they may also undergo slight breakage, whereas the other particles, which suffer from serious breakage and fail to fall in their original size range, are called broken particles.

As particles can be distinguished by their different colors, the PSD from the same-sized parent particles can be investigated, which is not found in previously published studies. Fig. 8a shows the PSDs before and after tests U1-U5, whereas Fig. 8b and Fig. 8c show the PSDs of the whole sample (PSD-W) and of the particles of each color (PSD-E) before and after tests M1 and M2, respectively, both on semi-log axes and on double-log axes. The PSD-Es of the particles of the same color in test M1, M2 and U1-U5 have different gradients, because they have different amounts of breakage. It is found that the PSDs obtained from tests U1-U5 are relatively linear in shape on the double-log plot (Fig. 8(a-2)), hence giving a clear fractal dimension at the end of the tests, in which the fractal dimension of the grey particles (U1) is the highest because they



have undergone more generations of breakage compared to that of other particles. However, for both tests M1 and M2, the PSD-Es are concave in shape (Fig. 8(b-2) and Fig. 8(c-2)) and below their respective uniformly graded PSDs in Fig. 8(a-2) because there is generally less breakage for each color when compared to U1-U5. This phenomenon is clearer for the larger parent particles (e.g. grey and green particles). When the applied vertical stress of M1 increases to 12.8 MPa, the PSD-Es in Fig. 8(b-2) become more linear in shape.

The particle breakage can be further investigated if it can be quantified. In the literature, the amount of breakage is usually evaluated by Hardin's relative breakage index (1985) or Einav's modified breakage index (2007), but it is not easy to apply these indexes in situations when there are missing portions of the PSDs for particles smaller than 2.0 mm and when the ultimate fractal dimension is unknown. In the next section, the particle breakage in the assembly is analyzed from the perspective of the mass survival probability.

### **Mass Survival Probability**

The survival probability of particles is usually calculated by the number of particles. As it is difficult to count the number of particles in assemblies, an alternative index called the mass survival probability is proposed, which is defined as

$$P_{ms} = m_s / m_o \quad (2)$$

where  $m_s$  is the mass of the surviving particles; and  $m_o$  is the mass of the particles before the test. By definition,  $1 - P_{ms}$  is the breakage probability, indicating the absolute breakage amount.

Fig. 9 shows the mass survival probability of particles with different initial sizes at the end of the oedometer tests. It can be seen that the mass survival probability is unequal for different-sized particles in M1 at 6.4 MPa. The largest particles (Grey<sub>BT-15.9</sub>) show the highest survival probability, while the medium-sized particles (Red<sub>BT-6.3</sub>) show the lowest survival probability. This phenomenon, which is also found in M1 at 3.2 MPa and 12.8 MPa (Fig. 9(b)) and M2 at 6.4 MPa (Fig. 9(a)), is attributed to the combined effects of the single-particle crushing strength and the coordination number, as illustrated in Fig. 10. The single-particle

crushing strength is negatively correlated with the particle size because smaller particles generally have fewer flaws than those of the larger particles (McDowell and Bolton 1998; Nakata et al. 1999). Since uniform particles have approximately the same coordination number (see inserts a and b in Fig. 10), their survival probability is mainly determined by the intrinsic crushing strength. In polydisperse samples, larger particles tend to have higher coordination numbers than those of smaller particles, so they exhibit more dispersed contact forces and lower deviatoric stress inside the particle, as demonstrated by Minh and Cheng (2013) and Shen et al. (2017). Thus, a high coordination number is beneficial to the survival of a particle. This is also described as the protective effect by surrounding particles in Palmer and Sanderson's literature (1991). Therefore, the particle crushing strength and the coordination number have opposite effects on the survival probability of particles. The combined effects of the two variables lead to relatively low survival probabilities for medium-sized particles and high survival probabilities for larger particles. From Fig. 9(b), it can be seen that with increasing applied vertical stress, the increase in the breakage probability of the largest particles slows down, indicating that the protective effect of the smaller particles on the larger particles is enhanced during particle breakage. In fact, it is found that the breakage of uniform particles can hardly reach 100% even under very high stresses (Hagerty et al. 1993; Shen et al. 2018).

In addition, it can be found in Fig. 9(a) that the mass survival probability of the particles is not only related to the particle size but is also dependent on the initial PSD. One example is that the mass survival probability of larger particles (Grey<sub>BT-15.9</sub> and Green<sub>BT-10.0</sub>) in polydisperse samples (M1 and M2) is much higher than that in the uniformly graded samples (U1-U5). This is because there are more smaller particles in polydisperse samples protecting the larger ones (see insert a and c in Fig. 10). Another example is that the mass survival probability of particles of the same size in M2 is higher than in M1 because adding 2.5 mm particles further increases the coordination numbers in M2 (see insert c and e in Fig. 10). Therefore, we can reasonably speculate that if more small particles are introduced to the PSD, the survival probability of the particles will further increase until reaching an arrangement state where all the particles are neighbored by a certain number of different-sized particles. This, in fact, describes the process of particle crushing in which

the generation of smaller fragments reduces the probability of breakage and slows down the particle crushing phenomenon. Regardless of the initial PSD, the particles are not ground down into fines, but always form a self-similar arrangement that is composed of particles with multigenerational sizes, also known as the fractal distribution (Palmer and Sanderson 1991; McDowell et al. 1996; McDowell & Bolton 1998; Coop et al. 2004; Ben-Nun et al. 2010; Altuhafi and Coop 2011). In summary, the survival probability of particles, especially of large particles, in the assembly is greatly affected by the particle-size-related coordination number. Unlike the particle crushing strength, which is an intrinsic and unchangeable property for particles, the coordination numbers could be easily adjusted by changing the PSD.

Fig. 11(a) shows the mass percentage of the particles of different size ranges/colors in M1 at 6.4 MPa. All size ranges experience a reduction in the particle mass through breakage into smaller sizes and also an increase in the particle mass broken from larger sizes, except the largest size range. The largest size range has the lowest mass percentage (15.9 mm grey bar) among the four size ranges, although its mass survival probability is the highest; however, smaller size ranges do not lose much mass despite their low survival probability, because they can gain fragments broken from larger particles. This reveals that the actual breakage amount can be far greater than what is observed in conventional particle crushing tests. The proportions of surviving particles and broken particles are labeled in each bar in Fig. 11. Smaller size ranges contain more broken particles. For particles in the 5.0-3.1 mm size range ( $d_0=4.0$  mm) at 6.4 MPa, 62% of them are surviving particles, while the other 38% are broken from larger size ranges. When the vertical stress reaches 12.8 MPa (Fig. 11(b)), the mass percentage of the broken particles increases to as high as 56%, showing that more particle breakage of the larger sizes has occurred. Meanwhile, a question arises as to whether the newly migrated particles can change the crushability of particles within a given size range, as they make up a large proportion of the total number of particles.

### ***Shape Characteristics of Test M1***

In this section, the shape characteristics of the particles in test M1 at 6.4 MPa were analyzed and compared with those of the original particles. The shape factors of the particles after the test still obey the Weibull distribution, with  $R^2 > 0.966$ . Table 5 shows their overall characteristic values and Weibull moduli within different size ranges.

Fig. 12 shows the changes in the overall shape characteristics between children and parent particles in different size ranges. Fig. 12(a) shows that the characteristic shape factors of the large particles seem to increase, whereas the characteristic shape factors of the small particles seem to decrease. Fig. 12(b) shows that the Weibull moduli of all the shape factors increase compared with the original value, meaning that the variability of the particle shape seems to decrease after compression. These trends are difficult to clearly explain and are not similar to those of other published tests (Yan and Shi 2014; Altuhafi and Coop 2016; Zhang et al. 2018). In fact, their test results are not consistent, either. As it is difficult to determine a consistent evolution trend of the overall particle shape for a certain size range, more detailed investigations are performed below.

Table 6 shows the characteristic value and Weibull modulus of the children particles of each color within each size range (i.e. particles of each size and color in Fig. 7). Results are mainly discussed in terms of the following two aspects:

(1) Different-sized children particles generated from the same-sized parents (Grey<sub>BT-15.9</sub>), as shown in Fig. 13;

(2) Same-sized children particles (4.0 mm) generated from different-sized parents, as shown in Fig. 14.

In Fig. 13(a), the solid lines with square marks represent children particles generated from the same-sized parents Grey<sub>BT-15.9</sub>, and the dashed lines with round marks represent corresponding sized parent particles for comparison. From the solid lines, it can be seen that the characteristic values ( $x_0$ ) of all the shape factors decrease with decreasing size of the children particles, and the trend appears to be more obvious compared to that of Fig. 12(a), although the characteristic values of  $C_x$  and  $S$  vary in a very narrow range (0.9-1.0). This means that smaller children particles generally lead to less convex, less spherical-like, more elongated and

flatter particle shapes. Suffering from repeated catastrophic fracture, small children particles tend to have winding outlines and bumpy surfaces, reflected in their low values for  $Cx$  and  $S$ . Compared with  $Cx$  (0.951-0.980) and  $S$  (0.901-0.940), the values of  $AR$  (0.712-0.799) and  $Fn$  (0.380-0.592) show more noticeable changes. In particular, the value of the flatness factor  $Fn$  shows a maximum difference of 56%, mainly because most of the small children particles are generated from the spalling of parent particles and usually the spalling fragments are sheet-like or acicular shaped.

In addition, by comparing the square marks and the round marks in Fig. 13(a), it is observed that the surviving particles have higher shape factors than their parents (e.g., Grey<sub>AT-15.9</sub> compared to Grey<sub>BT-15.9</sub>), while the broken particles generally have lower shape factors than the same-sized particles before the test (e.g., Grey<sub>AT-4.0</sub> compared to Yellow<sub>BT-4.0</sub>). It is worth recalling that some of the so-called “surviving” particles may be subjected to abrasion and corner wear, whose sizes after the tests still fall in the original size range despite the slight change in shape. During the abrasion of asperities, the convex parts of the particles are polished, leading to the reduction in the concave area and the perimeter of the particles. This directly causes an increase in the convexity and sphericity of the surviving particles, and changes the aspect ratio and flatness. This polishing effect is more conspicuous for larger particles that are encircled by more particles in the polydisperse granular assembly, such as Grey<sub>BT-15.9</sub>. With respect to the broken particles, they degrade not only in particle size, but also in particle shape, especially for the flatness factor (e.g., Grey<sub>AT-4.0</sub> compared to Yellow<sub>BT-4.0</sub>,  $Fn$  changes from 0.541 to 0.380, with a reduction of approximately 30%).

Fig. 13(b) shows that the trend of  $k$  with the change in the particle size is also obviously smaller (i.e., higher variability) for the smaller children particles, which cannot be seen clearly in Fig. 12(b). This can possibly be explained as follows. The shape factors of the surviving particles generally increase and their variabilities decrease because their surfaces are polished by abrasion and the poorly shaped particles are eliminated; the broken particles undergo various crushing processes, such as spalling, peeling, and splitting, and their shape factors have a tendency to be more irregular, so that the distribution range becomes wide.

Combining Fig. 13(a) and (b), it can be concluded that the improvement of the particle shape is usually accompanied by a narrowing down in the distribution range of shape factors.

In Fig. 14, the solid lines with square marks represent 4.0 mm children particles generated from different-sized parents, and the dashed lines with round marks represent their corresponding parent particles. Even though these children particles of different origins fall in the same size range, their shape factors show significant difference. Among the four groups of particles, Yellow<sub>AT-4.0</sub> has the highest value for both  $x_0$  and  $k$ , which is also higher than the value of their parent particles, because they are surviving particles. However, the values of  $x_0$  and  $k$  for the other three broken particle groups are generally lower than their parents and generally decrease with increasing parent size because smaller particles may have gone through several generations of breakage. These changes are more noticeable for the factor  $F_n$  than for other factors, which is the same as that observed in Fig. 13.

In summary, surviving particles have higher characteristic shape factors and narrower distribution ranges of the shape factors than their parents, while broken particles have lower characteristic shape factors and wider distribution ranges of the shape factors than their parent particles. Moreover, for children particles with the same sizes, the larger the size of their parents, the lower the characteristic shape factor and the wider the distribution range of the shape factor. These changes in shape may lead to the result that the single-particle crushing statistics of the parent particles are not applicable to the children particles, because they are not similar in geometry. We could reasonably speculate that surviving particles would have higher chance of remaining intact compared with broken particles of the same size. In this context, the influence of the breakage-induced shape irregularity on particle crushing statistics should be considered.

Now, it is clear why we cannot find a consistent shape evolution in conventional experimental tests when analyzing the changes in the shape factors of the overall particles within a certain size range. From Fig. 13 and Fig. 14, we find that some particles (usually surviving particles) exhibit an increase in their shape factors, while the other particles (usually broken particles) experience a decrease. As the overall shape factors of the particles within a certain size range (Fig. 12) are the weighted results of the surviving particles and

broken particles, which depend on the quantity ratio of the two parts, the changing trends of the overall particle shapes are therefore uncertain.

### **Influence of Breakage-induced Shape Irregularity on the Oedometer Survival Probability**

It is clearly demonstrated in the previous section that the same-sized children particles from different-sized parents have different particle shapes. How the difference in the particle shape will in turn influence the particle crushing statistics remains unclear. In this section, we will explore how the particle shape affects the survival probability. The particles tested were 4.0 mm children particles of M1 at 6.4 MPa (i.e., Grey<sub>AT-4.0</sub>, Green<sub>AT-4.0</sub>, Red<sub>AT-4.0</sub>, and Yellow<sub>AT-4.0</sub>), whose shapes were significantly different, as mentioned above. The most straightforward way to test their survival probability is to carry out single-particle crushing tests between two flat rigid plates (McDowell and Bolton 1998; Nakata et al. 1999; Cheng et al. 2003), but since some of the particles are too flat (e.g., Grey<sub>AT-4.0</sub>), the orientation of the particles may be a governing factor that affects the test results. Hence, this method was not adopted here. Inspired by Nakata et al. (2001), who once seeded a few dyed particles in oedometer and triaxial samples to observe their crushing characteristics, the survival probability of the particles in this study was determined by embedding individual particles in an assembly of the original 4.0 mm white gypsum particles inside an oedometer. The test program is listed in Table 7. Twenty particles were tested under each vertical stress (0.8, 1.6, 3.2, 6.4, 12.8, and 25.6 MPa). The diameter of the oedometer cell is 50 mm, and each sample weighed 40 g, with an initial void ratio of 1.39.

Note that the survival probability  $P_{ns}$  in this section is calculated by the number of particles, which is given by,

$$P_{ns} = n_s / n_o \quad (3)$$

where  $n_s$  is the number of surviving particles, and  $n_o$  is the number of the particles tested, with  $n_o = 20$ . Fig. 15(a) shows the survival probability of various particles under different vertical stresses. Clear differences in the magnitude of  $P_{ns}$  at the same stress level can be observed, i.e., Yellow<sub>AT-4.0</sub> > Red<sub>AT-4.0</sub> >

Green<sub>AT-4.0</sub> > Grey<sub>AT-4.0</sub>. To quantitatively compare their differences, the Weibull distribution function is used to describe the survival probability of the granular materials during particle crushing, which is given by

$$P_{ns}(\sigma_v) = \exp\left[-\left(\frac{\sigma_v}{\sigma_{v0}}\right)^k\right] \quad (4)$$

where  $\sigma_{v0}$  is the characteristic vertical stress of 37% of particles surviving;  $\sigma_v/\sigma_{v0}$  is the normalized vertical stress; and  $k$  is the Weibull modulus reflecting the variable range of the stress. Table 8 shows the curve fitting results. Fig. 15(b) shows the survival probability against the normalized vertical stress.

There is no significant difference in the values of the Weibull modulus between the different particles. This is because the Weibull modulus is a material constant that is only related to the mineralogy of the grains. However, the characteristic vertical stress of Yellow<sub>AT-4.0</sub> is almost three times higher than that of Grey<sub>AT-4.0</sub>, probably because the Grey<sub>AT-4.0</sub> particles are more irregular in shape than the Yellow<sub>AT-4.0</sub> particles. Fig. 16 shows that the characteristic vertical stress increases with increasing characteristic shape factors and decreasing distribution range of the shape factors, indicating that the survival chances for the irregular particles undergoing external stresses are substantially lower than those for the regular particles. If one further considers the cause of the difference in the particle shape, it can be concluded that particle crushing changes the shape of the particles, and the breakage-induced shape irregularity, in turn, influences the survival probability of the particles.

## Conclusions

In this paper, artificial dyed gypsum particles (DGPs) were used to study the survival probability and shape evolution of crushable particles during 1D compression. The main work and findings are summarized as follows:

a) The  $e - \log \sigma_v$  curves of the DGP samples show obvious bilinearity and yield points as conventional granular materials, indicating that the DGPs can be used to reflect the mechanical response of granular soils. Compared with conventional granular materials, the use of DGPs allows us to match the children particles to



their parents so that more detailed studies can be carried out on particle crushing. By acquiring the image of the individual particles from the top and the side, we can further quantitatively analyze the particle shape factors (the Feret diameters, convexity, sphericity, aspect ratio, and flatness) with a self-written MATLAB program. In addition, the PSDs of the DGPs can be obtained by the program.

b) The use of DGPs provides a possible method to obtain PSDs of particles of each color in the mixed-sized samples. The breakage amount of the particles is indicated by the mass survival probability. It is found that the fractional fracturing of the particles in the assembly is not only related to the particle size but also depends on the initial PSD. Larger particles in polydisperse samples have a much higher survival probability than in uniform samples, while medium-sized particles in polydisperse samples have the lowest survival probability. This is attributed to the combined effects of the particle crushing strength and the coordination number. In addition, although the small particles have a lower survival probability, their size range does not lose much particle mass even when compressed to 12.8 MPa because the small particles gain a great number of broken particles that migrate from the larger size ranges. This implies that the actual breakage amount is far greater than what is observed in conventional particle crushing experiments.

c) Two parameters in the Weibull distribution function, namely, the characteristic value ( $x_0$ ) and the distribution range ( $k$ ) are used to quantitatively characterize the shape of both the parent and children particles. It is found that the surviving particles, part of which are subjected to abrasion from the surrounding particles, tend to have higher values of convexity, sphericity, aspect ratio and flatness and narrower distribution range of these shape factors than the original particles; however, the shape factors of broken particles show totally opposite changing trends. In addition, the shape irregularity of children particles tends to increase with the size difference between them and their parents. The above phenomena are more noticeable for the flatness factor. Furthermore, the shape factors of particles after the test are the weighed values of the surviving particles and broken particles. Their changing trends are therefore uncertain.

d) By testing the oedometer survival probability of children particles of the same size generated from different parents, it is found that the Weibull modulus is independent of the particle shape, while the

characteristic crushing vertical stress increases with increasing characteristic shape factor and decreasing distribution range. This confirms that the breakage-induced shape irregularity does have an influence on the magnitude of the survival probability. In other words, the single-particle crushing statistics of the parent particles may no longer be applicable for the children particles.

### **Data availability statement**

All data, models, or code that support the findings of this study are available from the corresponding author upon reasonable request.

### **Acknowledgments**

This paper was supported by National Key R&D Program of China (Grant No. 2017YFC0404805), the Joint Funds of the National Natural Science Foundation of China (Grant Nos. U1765205; 51979091), and the Fundamental Research Funds for the Central Universities (Grant No. B200203017). The authors are also grateful to the anonymous reviewers for their excellent comments and suggestions.

## References

- Abbireddy, C.O.R., and Clayton, C.R.I. (2009). "A review of modern particle sizing methods." *Proceedings of the Institution of Civil Engineers - Geotechnical Engineering*, 162(4), 193–201.  
<https://doi.org/10.1680/geng.2009.162.4.193>
- Alonso, E.E., Tapias, M., and Gili, J. (2012). "Scale effects in rockfill behaviour." *Géotechnique Letters*, 2, 155–160. <https://doi.org/10.1680/geolett.12.00025>
- Altuhafi, F. N., Coop, M. R. (2011). Changes to particle characteristics associated with the compression of sands. *Géotechnique*, 61(6), 459–471. <https://doi.org/10.1680/geot.9.P.114>
- Altuhafi, F.N., Coop, M.R., and Georgiannou, V.N. (2016). "Effect of particle shape on the mechanical behavior of natural sands." *Journal of Geotechnical and Geoenvironmental Engineering*, 142(12), 04016071. [https://doi.org/10.1061/\(ASCE\)GT.1943-5606.0001569](https://doi.org/10.1061/(ASCE)GT.1943-5606.0001569)
- Altuhafi, F., O'Sullivan, C., and Cavarretta, I. (2013). "Analysis of an image-based method to quantify the size and shape of sand particles". *Journal of Geotechnical and Geoenvironmental Engineering*, 139(8), 1290-1307. [https://doi.org/10.1061/\(ASCE\)GT.1943-5606.0000855](https://doi.org/10.1061/(ASCE)GT.1943-5606.0000855)
- Barrett, P.J. (1980). "The shape of rock particles, a critical review." *Sedimentology*, 27, 291-303.  
<https://doi.org/10.1111/j.1365-3091.1981.tb01934.x>
- Ben-Nun, O., Einav, I., and Tordesillas, A. (2010). "Force attractor in confined comminution of granular materials". *Physical review letters*, 104(10), 108001.  
<https://doi.org/10.1103/PhysRevLett.104.108001>
- Cheng, Y.P., Nakata, Y., and Bolton, M.D. (2003). "Discrete element simulation of crushable soil". *Géotechnique*, 53(7), 633–641. <https://doi.org/10.1680/geot.2003.53.7.633>
- Cheng, Y.P., Bolton, M.D., and Nakata, Y. (2004). "Crushing and plastic deformation of soils simulated using DEM." *Géotechnique*, 54(2), 131–141. <https://doi.org/10.1680/geot.2004.54.2.131>

- China National Standards CNS-GB/T50123-1999. (1999). "Specification of Soil testtest." Standardization Administration of China (SAC), Ministry of Construction, Ministry of Water Resources, China Planning Press, Beijing.
- Cho, G.C., Dodds, J., and Santamarina, J.C. (2006). "Particle shape effects on packing density, stiffness, and strength, natural and crushed sand." *Journal of Geotechnical and Geoenvironmental Engineering*, 132(5), 591-602. [https://doi.org/10.1061/\(ASCE\)1090-0241\(2006\)132:5\(591\)](https://doi.org/10.1061/(ASCE)1090-0241(2006)132:5(591))
- Coop, M.R., Sorensen, K.K., Bodas-Freitas, T. and Georgoutsos, G. (2004). "Particle breakage during shearing of a carbonate sand." *Géotechnique*, 54(3), 157–163. <https://doi.org/10.1680/geot.2004.54.3.157>
- Einav, I. (2007). "Breakage mechanics-part I, theory." *Journal of the Mechanics and Physics of Solids*, 55(6), 1274–1297. <https://doi.org/10.1016/j.jmps.2006.11.003>
- Eliš, J. (2014). "Simulation of railway ballast using crushable polyhedral particles." *Powder Technology*, 264, 458–465. <https://doi.org/10.1016/j.powtec.2014.05.052>
- Ferrellec, J.-F., and McDowell, G.R. (2010). "A method to model realistic particle shape and inertia in DEM." *Granular Matter*, 12, 459–467. <https://doi.org/10.1007/s10035-010-0205-8>
- Gladkyy, A., and Kuna, M. (2017). "DEM simulation of polyhedral particle cracking using a combined Mohr–Coulomb–Weibull failure criterion." *Granular Matter*. <https://doi.org/10.1007/s10035-017-0731-8>
- Hagerty, M., Hite, D., Ullrich, C., and Hagerty, D. (1993). "One-dimensional high-pressure compression of granular media." *Journal of Geotechnical Engineering*, 119(1), 1–18. [https://doi.org/10.1061/\(ASCE\)0733-9410\(1993\)119:1\(1\)](https://doi.org/10.1061/(ASCE)0733-9410(1993)119:1(1))
- Hardin, B.O. (1985). "Crushing of soil particles." *Journal of Geotechnical Engineering*, 111(10), 1177–1192. [https://doi.org/10.1061/\(ASCE\)0733-9410\(1985\)111:10\(1177\)](https://doi.org/10.1061/(ASCE)0733-9410(1985)111:10(1177))

- Hurley, R.C., Hall, S.A., Andrade, J.E., and Wright, J. (2016). “Quantifying interparticle forces and heterogeneity in 3D granular materials.” *Physical Review Letters*, 117(9), 098005. <https://doi.org/10.1103/PhysRevLett.117.098005>
- Indraratna, B., Sun, Q.D., and Nimbalkar S. (2015). “Observed and predicted behavior of rail ballast under monotonic loading capturing particle breakage.” *Canadian Geotechnical Journal*, 52(1), 73–86. <https://doi.org/10.1139/cgj-2013-0361>
- Jardine, R.J., Zhu, B.T., Foray, P., and Yang, Z.X. (2013). “Interpretation of stress measurements made around closed-ended displacement piles in sand.” *Géotechnique*, 63(8), 613–627. <https://doi.org/10.1680/geot.9.P.138>
- Jia, X., and Williams, R.A. (2001). “A packing algorithm for particles of arbitrary shapes.” *Powder Technology*, 120, 175–186. [https://doi.org/10.1016/S0032-5910\(01\)00268-6](https://doi.org/10.1016/S0032-5910(01)00268-6)
- Jia, Y., Xu, B., Chi, S., Xiang, B., and Zhou, Y. (2017). “Research on the particle breakage of rockfill materials during triaxial tests.” *International Journal of Geomechanics*, 17(10), 04017085. [https://doi.org/10.1061/\(ASCE\)GM.1943-5622.0000977](https://doi.org/10.1061/(ASCE)GM.1943-5622.0000977)
- Kittu, A., Watters, M., Cavarretta, I., and Bernhardt-Barry, M.L. (2019). “Characterization of additive manufactured particles for DEM validation studies.” *Granular Matter*. <https://doi.org/10.1007/s10035-019-0908-4>
- Kong, L., Ostadhassan, M., Li, C., and Tamimi, N. (2018). “Can 3-D printed gypsum samples replicate natural rocks? An experimental study.” *Rock Mechanics and Rock Engineering*, 51(10), 3061–3074. <https://doi.org/10.1007/s00603-018-1520-3>
- Kong, L., Ostadhassan, M., Li, C., and Tamimi, N. (2018). “Pore characterization of 3D-printed gypsum rocks, a comprehensive approach.” *Journal of Materials Science*, 53(7), 5063–5078. <https://doi.org/10.1007/s10853-017-1953-1>
- Kwok, C.Y., and Bolton, M.D. (2013). “DEM simulations of soil creep due to particle crushing.” *Géotechnique*, 63(16), 1365–1376. <https://doi.org/10.1680/geot.11.P.089>

- Lade, P.V., Yamamuro, J.A., and Bopp, P.A. (1996). "Significance of particle crushing in granular materials." *Journal of Geotechnical Engineering*, 122(4), 309–316.  
[https://doi.org/10.1061/\(ASCE\)0733-9410\(1996\)122:4\(309\)](https://doi.org/10.1061/(ASCE)0733-9410(1996)122:4(309))
- Liu, S., Mao, H., Wang, Y., and Weng, L. (2018). "Experimental study on crushable coarse granular materials during monotonic simple shear tests." *Geomechanics and Engineering*, 15(1), 687-694.  
<https://doi.org/10.12989/gae.2018.15.1.687>
- Lu, M., and McDowell, G.R. (2010). "Discrete element modelling of railway ballast under monotonic and cyclic triaxial loading." *Géotechnique*, 60(6), 459–467. <https://doi.org/10.1680/geot.2010.60.6.459>
- Mao, W., Aoyama, S., and Towhata, I. (2019). "A study on particle breakage behavior during pile penetration process using acoustic emission source location." *Geoscience Frontiers*.  
<https://doi.org/10.1016/j.gsf.2019.04.006>
- Marsal, J. (1967). "Large-scale testing of rockfills materials." *Journal of the Soil Mechanics and Foundation Engineering*, 93(2), 27–44.
- McDowell, G. R. (2002). "On the yielding and plastic compression of sand". *Soils and Foundations*, 42(1), 139-145. <https://doi.org/10.3208/sandf.42.139>
- McDowell, G.R. and Bolton, M.D. (1998). "On the micromechanics of crushable aggregates." *Géotechnique*, 48(5), 667-679. <https://doi.org/10.1680/geot.1998.48.5.667>
- McDowell, G. R., Bolton, M. D., and Robertson, D. (1996). "The fractal crushing of granular materials". *Journal of the Mechanics and Physics of Solids*, 44(12), 2079–2102. [https://doi.org/10.1016/S0022-5096\(96\)00058-0](https://doi.org/10.1016/S0022-5096(96)00058-0)
- Minh, N.H. and Cheng, Y.P. (2013). "A DEM investigation of the effect of particle-sized distribution on one-dimensional compression." *Géotechnique*, 63(1), 44–53. <https://doi.org/10.1680/geot.10.P.058>
- Nakata, Y., A. Hyde, F.L., Hyodo, M., and Murata, H. (1999). "A probabilistic approach to sand particle crushing in the triaxial test." *Géotechnique*, 49(5), 567-583.  
<https://doi.org/10.1680/geot.1999.49.5.567>

- Nakata, Y., Hyodo, M.A., Hyde, F.L., Kato, Y., and Murata, H. (2001). "Microscopic particle crushing of sand subjected to high pressure one-dimensional compression." *Soils and Foundations*, 41(1), 69-82. <https://doi.org/10.3208/sandf.41.69>
- Obaidat, M.T., Ghuzlan, K.A., and Alawneh, M.M. (2017). "Analysis of volumetric properties of bituminous mixtures using cellular phones and image processing techniques." *Canadian Journal of Civil Engineering*, 44(9), 715–726. <https://doi.org/10.1139/cjce-2017-0085>
- Palmer, A.C., & Sanderson, T.J.O. (1991). "Fractal crushing of ice and brittle solids". *Proceedings of the Royal Society of London. Series A: Mathematical and Physical Sciences*, 433(1889), 469-477. <https://doi.org/10.1098/rspa.1991.0060>
- Peng, Y., Ding, X., Xiao, Y., Deng, X., and Deng, W. (2019). "Detailed amount of particle breakage in non-uniformly graded sands under one-dimensional compression." *Canadian Geotechnical Journal*. <https://doi.org/10.1139/cgj-2019-0283>
- Prudêncio, L.R., Weidmann, D.F., de Oliveira, A.L., and Damo, G.F. (2013). "Particle shape analysis of fine aggregate using a simplified digital image processing method." *Magazine of Concrete Research*, 65(1), 27–36. <https://doi.org/10.1680/macr.11.00199>
- Shen, C.M., Liu, S.H., Wang, L.J., and Wang, Y.S. (2019). "Micromechanical modeling of particle breakage of granular materials in the framework of thermomechanics." *Acta Geotechnica*, 14(4), 939–954. <https://doi.org/10.1007/s11440-018-0692-z>
- Shen, C.M., Liu, S.H., and Wang, Y.S. (2017). "Microscopic interpretation of one-dimensional compressibility of granular materials." *Computers and Geotechnics*, 91, 161-168. <https://doi.org/10.1016/j.compgeo.2017.07.010>
- Sun, Q.D., Indraratna, B., and Nimbalkar, S. (2016). "Deformation and degradation mechanisms of railway ballast under high frequency cyclic loading." *Journal of Geotechnical and Geoenvironmental Engineering*, 142(1), 04015056. [https://doi.org/10.1061/\(ASCE\)GT.1943-5606.0001375](https://doi.org/10.1061/(ASCE)GT.1943-5606.0001375)

- Suzukia, M., Shinmurab, T., Iimuraa, K., and Hirotaa, M. (2008). "Study of the wall effect on particle packing structure using x-ray micro computed tomography." *Advanced Powder Technology*, 19, 183–195. <https://doi.org/10.1163/156855208X293817>
- Tapias, M., Alonso, E.E., and Gili, J. (2015). "A particle model for rockfill behavior." *Géotechnique*, 65(12), 975–994. <https://doi.org/10.1680/jgeot.14.P.170>
- Walton, W.H. (1948). "Feret's statistical diameter as a measure of particle size." *Nature*, 162(4113), 329-330. <https://doi.org/10.1038/162329b0>
- Wang, B., Martin, U., and Rapp, S. (2017). "Discrete element modelling of the single-particle crushing test for ballast stones." *Computers and Geotechnics*, 88, 61–73. <https://doi.org/10.1016/j.compgeo.2017.03.007>
- Wang T., Liu S.H., Feng Y., and Yu J.D. (2018). Compaction characteristics and minimum void ratio prediction model for gap-graded soil-rock mixture. *Applied Sciences*, 8(12), 2584. <https://doi.org/10.3390/app8122584>
- Weibull, W., Stockholm, and Sweden. (1951). "A statistical distribution function of wide applicability." *Journal of Applied Mechanics*, 13, 293-297.
- Wiebicke, M., Andò, E., Herle, I., and Viggiani, G. (2017). "On the metrology of interparticle contacts in sand from x-ray tomography images". *Measurement Science and Technology*, 28(12), 124007. <https://doi.org/10.1088/1361-6501/aa8dbf>
- Wood, D.M., and Maeda, K. (2008). "Changing grading of soil, effect on critical state." *Acta Geotechnica*, 3(1), 3–14. <https://doi.org/10.1007/s11440-007-0041-0>
- Wu, Z., Zhang, B., Weng, L., Liu, Q., and Wong, LNY. (2019). "A new way to replicate the highly stressed soft rock, 3d printing exploration." *Rock Mechanics and Rock Engineering*. <https://doi.org/10.1007/s00603-019-01926-1>



- Xiao, Y., Liu, H., Ding, X., Chen, Y., Jiang, J., and Zhang, W. (2016). "Influence of particle breakage on critical state line of rockfill material." *International Journal of Geomechanics*, 16(1), 04015031. [https://doi.org/10.1061/\(ASCE\)GM.1943-5622.0000538](https://doi.org/10.1061/(ASCE)GM.1943-5622.0000538)
- Xiao, Y., Meng, M., Daouadji, A., Chen, Q., Wu, Z., and Jiang, X. (2018). "Effects of particle size on crushing and deformation behaviors of rockfill materials." *Geoscience Frontiers*. <https://doi.org/10.1016/j.gsf.2018.10.010>
- Yan, W.M., and Shi, Y. (2014). "Evolution of grain grading and characteristics in repeatedly reconstituted assemblages subject to one-dimensional compression." *Géotechnique Letters*, 4(3), 223–229. <https://doi.org/10.1680/geolett.14.00039>
- Yang, H., Zhou, B., and Wang, J. (2019). "Exploring the effect of 3D grain shape on the packing and mechanical behaviour of sands." *Géotechnique Letters*. <https://doi.org/10.1680/jgele.18.00227>
- Zhang, X., Hu, W., Scaring, G., Baudet, B.A., and Han, W. (2018). "Particle shape factors and fractal dimension after large shear strains in carbonate sand." *Géotechnique Letters*, 8(1), 73–79. <https://doi.org/10.1680/jgele.17.00150>

**Table 1** Material properties of the gypsum powder

Property	Value
Whiteness	92
Fineness	200
Powder-water-dye ratio	1:0.34:0.02
Initial setting time	8 min
Demolding time	30 min
Curing temperature	20 °C
Curing time	24 h
2-hour flexural strength	7 MPa

**Table 2** Mean value of the shape factors of parent particles

Test particle	Number	Size range (mm)	$d_0$ (mm)	$C_x$	$S$	$AR$	$Fn$
Grey <sub>BT-15.9</sub> *	200	20.0-12.6	15.9	0.961	0.908	0.713	0.505
Green <sub>BT-10.0</sub>	200	12.6-7.9	10.0	0.956	0.909	0.720	0.511
Red <sub>BT-6.3</sub>	200	7.9-5.0	6.3	0.954	0.921	0.715	0.509
Yellow <sub>BT-4.0</sub>	200	5.0-3.1	4.0	0.946	0.933	0.710	0.499
Blue <sub>BT-2.5</sub>	200	3.1-2.0	2.5	0.949	0.938	0.711	0.501

\* For the sake of convenience, particles of different colors and sizes before and after tests are denoted as the uniform format: Color<sub>BT/AT-size</sub>, where “Color” indicates the color of the particle; “BT” and “AT” mean “before the test” and “after the test”, respectively; and “size” reflects the characteristic size  $d_0$  of the particle. For example, Grey<sub>BT-15.9</sub> represents the grey particles before the test with the characteristic size of 15.9 mm.

**Table 3** Weibull distribution parameters of the shape factors of parent particles

Test particle	$C_x$		$S$		$AR$		$Fn$	
	$C_{x0}$	$k$	$S_0$	$k$	$AR_0$	$k$	$Fn_0$	$k$
Grey <sub>BT-15.9</sub>	0.969	78.3	0.922	33.7	0.751	8.8	0.547	5.0
Green <sub>BT-10.0</sub>	0.964	70.9	0.925	29.5	0.760	8.5	0.552	5.1
Red <sub>BT-6.3</sub>	0.962	74.7	0.937	32.0	0.758	7.7	0.550	4.6
Yellow <sub>BT-4.0</sub>	0.956	65.8	0.943	30.8	0.754	7.8	0.541	5.3
Blue <sub>BT-2.5</sub>	0.958	69.9	0.954	30.9	0.755	7.6	0.545	4.9

**Table 4** Initial PSDs, initial void ratios, and compressibility indexes of the DGP samples for one-dimensional compression tests

Test ID	Mass of the DGPs of each size range (g)					Total mass (g)	$e_0$	$C_c$
	Grey <sub>BT-15.9</sub>	Green <sub>BT-10.0</sub>	Red <sub>BT-6.3</sub>	Yellow <sub>BT-4.0</sub>	Blue <sub>BT-2.5</sub>			
M1	150	150	150	150	-	600	1.266	0.527
U1	600	-	-	-	-	600	1.506	0.673
U2	-	600	-	-	-	600	1.454	0.657
U3	-	-	600	-	-	600	1.405	0.642
U4	-	-	-	600	-	600	1.378	0.623
U5	-	-	-	-	600	600	1.371	0.610
M2	120	120	120	120	120	600	1.175	0.427

**Table 5** Weibull distribution parameters of the shape factors of the overall children particles within different size range

Test particle	$Cx$		$S$		$AR$		$Fn$	
	$Cx_0$	$k$	$S_0$	$k$	$AR_0$	$k$	$Fn_0$	$k$
AT-15.9	0.980	138.1	0.940	44.6	0.799	10.6	0.592	5.6
AT-10.0	0.972	9.3	0.935	36.7	0.772	83.7	0.571	5.8
AT-6.3	0.968	76.9	0.927	34.6	0.749	9.1	0.548	5.4
AT-4.0	0.963	65.5	0.924	32.0	0.745	8.3	0.521	5.54

**Table 6** Weibull distribution parameters of the shape factors of the children particles in each color within different size ranges

Test particle	Number	Cx		S		AR		Fn	
		$Cx_0$	$k$	$S_0$	$k$	$AR_0$	$k$	$Fn_0$	$k$
Grey <sub>AT-15.9</sub>	48	0.980	138.1	0.940	44.6	0.799	10.6	0.592	5.6
Grey <sub>AT-10.0</sub>	46	0.971	80.5	0.916	38.1	0.732	8.5	0.523	5.0
Green <sub>AT-10.0</sub>	109	0.970	84.0	0.932	35.5	0.746	9.1	0.587	6.1
Grey <sub>AT-6.3</sub>	46	0.960	56.7	0.908	25.3	0.719	7.0	0.454	3.2
Green <sub>AT-6.3</sub>	112	0.963	63.0	0.919	34.0	0.764	9.6	0.505	5.2
Red <sub>AT-6.3</sub>	112	0.960	56.7	0.908	25.3	0.719	7.0	0.573	5.7
Grey <sub>AT-4.0</sub>	111	0.951	42.4	0.901	22.4	0.712	6.4	0.380	2.9
Green <sub>AT-4.0</sub>	112	0.957	45.9	0.906	20.7	0.689	6.1	0.395	3.8
Red <sub>AT-4.0</sub>	112	0.960	60.0	0.916	26.4	0.727	7.2	0.475	4.8
Yellow <sub>AT-4.0</sub>	112	0.966	71.5	0.930	36.3	0.761	9.1	0.564	6.2

**Table 7** test program for the oedometer survival probability of the same-sized children particles generated from different-sized parents

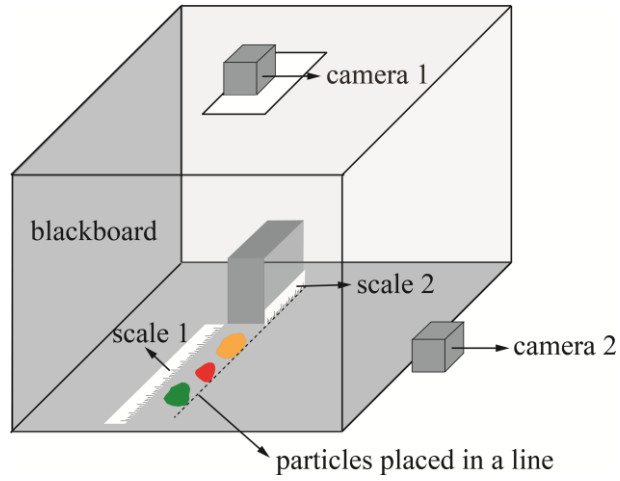
Test parameter/variable	Value/Range
Size of the surrounding particles	5.0-3.1 mm ( $d_0=4.0$ mm)
Color of the surrounding particles	white
Diameter of the sample	50 mm
Mass of the sample	40 g
Initial void ratio	1.39
Vertical stress level	0.8, 1.6, 3.2, 6.4, 12.8, and 25.6 MPa
Number of the particles tested	20 under each stress level

**Table 8** Curve fitting results of the oedometer survival probability using Weibull distribution function

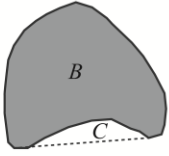
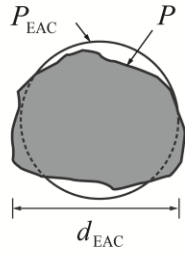
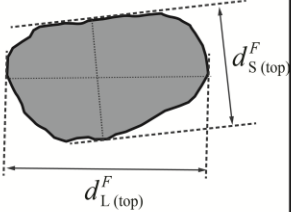
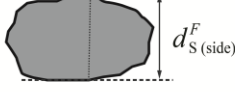
Test particle	$\sigma_{v0}$ (MPa)	$k$
Grey <sub>AT-4.0</sub>	3.90	1.15
Green <sub>AT-4.0</sub>	5.49	1.17
Red <sub>AT-4.0</sub>	8.03	1.15
Yellow <sub>AT-4.0</sub>	11.95	1.13



**Fig. 1.** (a) Manufactured dyed gypsum boards; (b) dyed gypsum particles (DGPs) (parent particles)



**Fig. 2.** The schematic diagram of particle shape measurement

Top projection			Side projection
$Cx$	$S$	$AR$	$Fn$
			
$Cx = \frac{B}{B+C}$	$S = \frac{P_{EAC}}{P} = \frac{2\sqrt{\pi A}}{P}$	$AR = \frac{d_{S(top)}^F}{d_{L(top)}^F}$	$Fn = \frac{d_{S(side)}^F}{d_{L(top)}^F}$

$P$ —perimeter;  $A$ —area; EAC—equivalent area circle;  $P_{EAC}$ —perimeter of the equivalent area circle;  $d_{EAC}$ —diameter of the equivalent area circle;  $d_{S(top)}^F$ —short-size Feret diameter of the top projection;  $d_{L(top)}^F$ —long-size Feret diameter of the top projection;  $d_{S(side)}^F$ —short-size Feret diameter of the side projection;

**Fig. 3.** Definitions of convexity ( $Cx$ ), sphericity ( $S$ ), aspect ratio ( $AR$ ) and flatness ( $Fn$ )

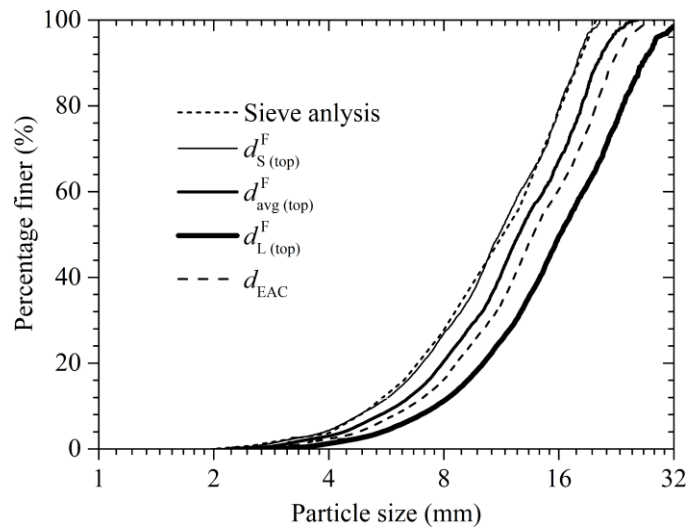


**Fig. 4.** Comparison of different PSDs of a polydisperse DGP sample

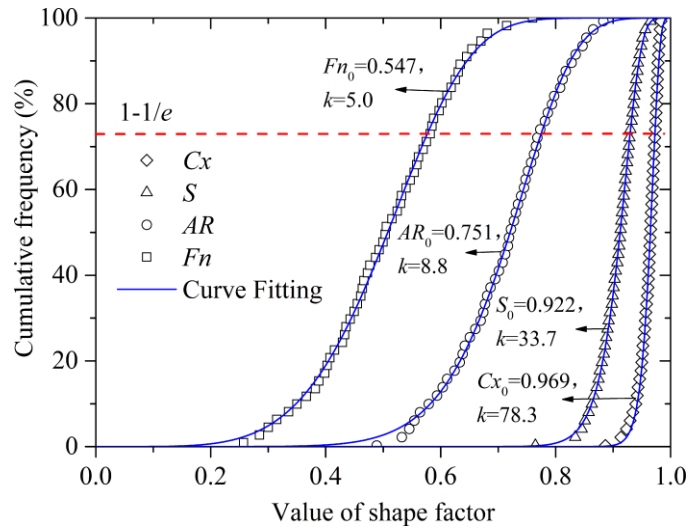


**Fig. 5.** Distributions of shape factors of parent particles (Grey<sub>BT-15.9</sub>) and the fitted curves using Weibull distribution function

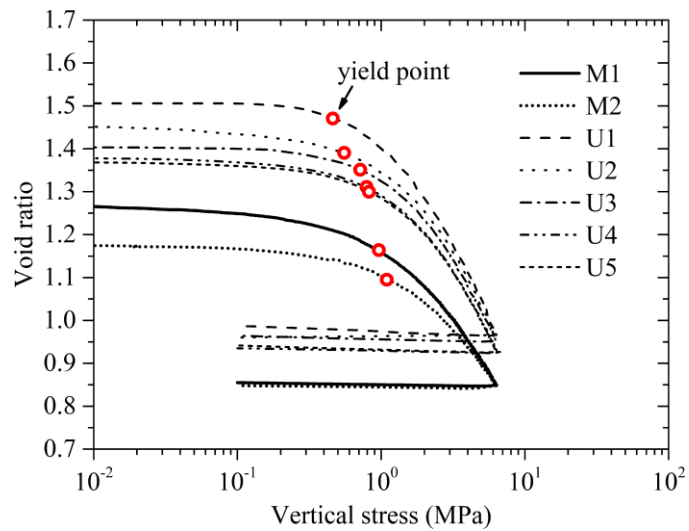


**Fig. 6.**  $e \sim \lg \sigma_v$  curve of DGPs during 1D compression tests

$d_0$ : mm	15.9		10.0		6.3		4.0		<3.1
Size range	20.0-15.9	15.9-12.6	12.6-10.0	10.0-7.9	7.9-6.3	6.3-5.0	5.0-4.0	4.0-3.1	
Grey <sub>AT</sub>									too small to pick out
Green <sub>AT</sub>	survived particles								
Red <sub>AT</sub>									
Yellow <sub>AT</sub>					survived particles				

**Fig. 7.** The DGPs separated according to their sizes and colors after Test M1



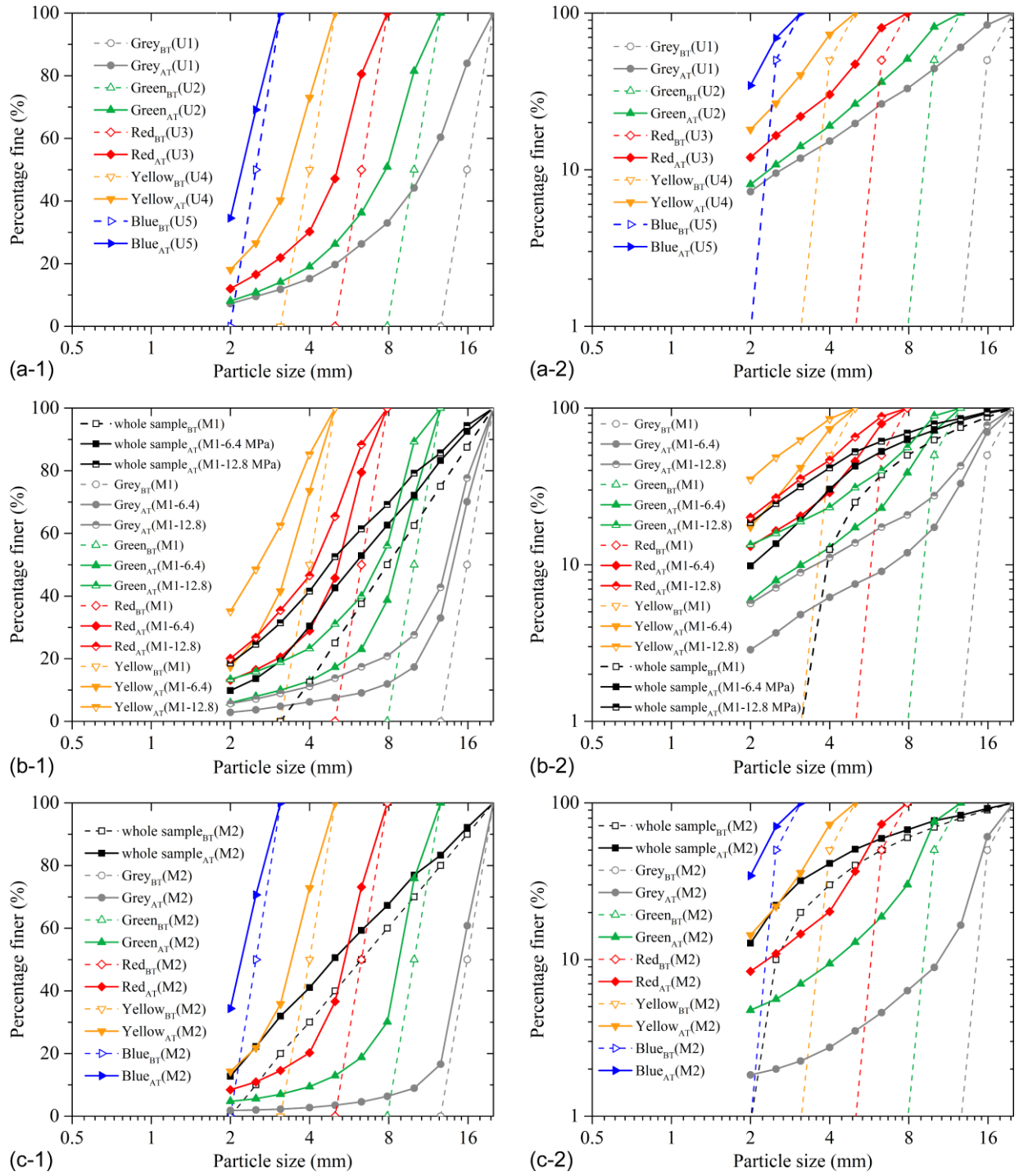


**Fig. 8.** PSDs of whole samples and of each-color particles before and after tests (a-1) U1-U5 at 6.4 MPa on semi-log axes; (a-2) U1-U5 at 6.4 MPa on double-log axes; (b-1) M1 at 6.4 MPa and 12.8 MPa on semi-log axes; (b-2) M1 at 6.4 MPa and 12.8 MPa on double-log axes; (c-1) M2 at 6.4 MPa on semi-log axes; (c-2) M2 at 6.4 MPa on double-log axes

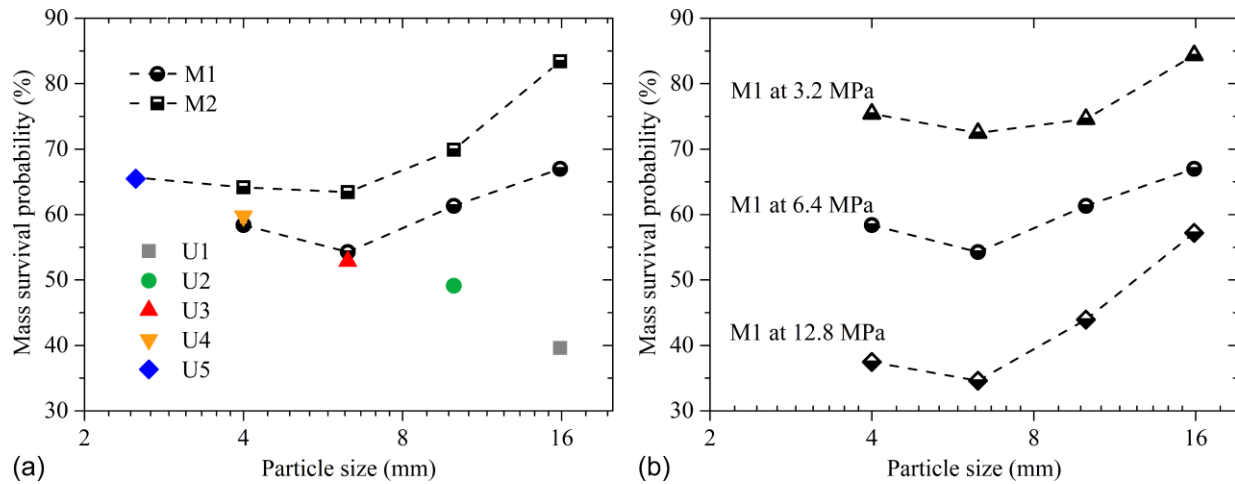


**Fig. 9.** Mass survival probability of particles at the end of oedometer tests (a) M1, M2 and U1-U5 at 6.4 MPa; (b) M1 at 3.2, 6.4, 12.8 MPa

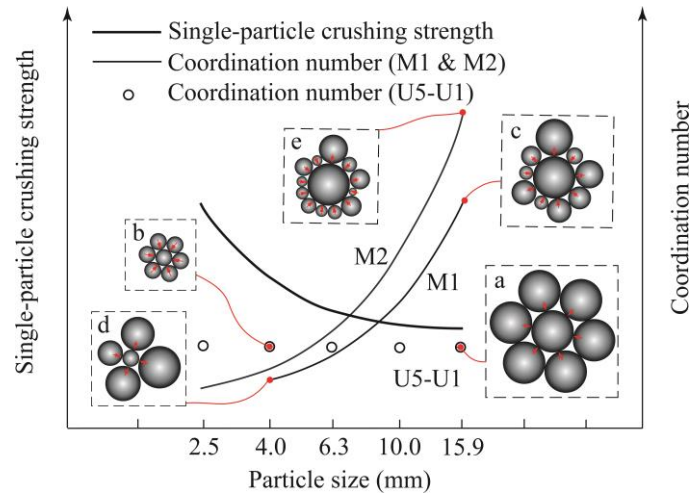


**Fig. 10.** Conceptual interpretation of the combined effects of the particle crushing strength and the coordination number on the surviving probability of particles in assemblies (a) 15.9 mm particles in U1; (b) 4.0 mm particles in U4; (c) 15.9 mm particles in M1; (d) 4.0 mm particles in M1; (e) 15.9 mm particles in M2

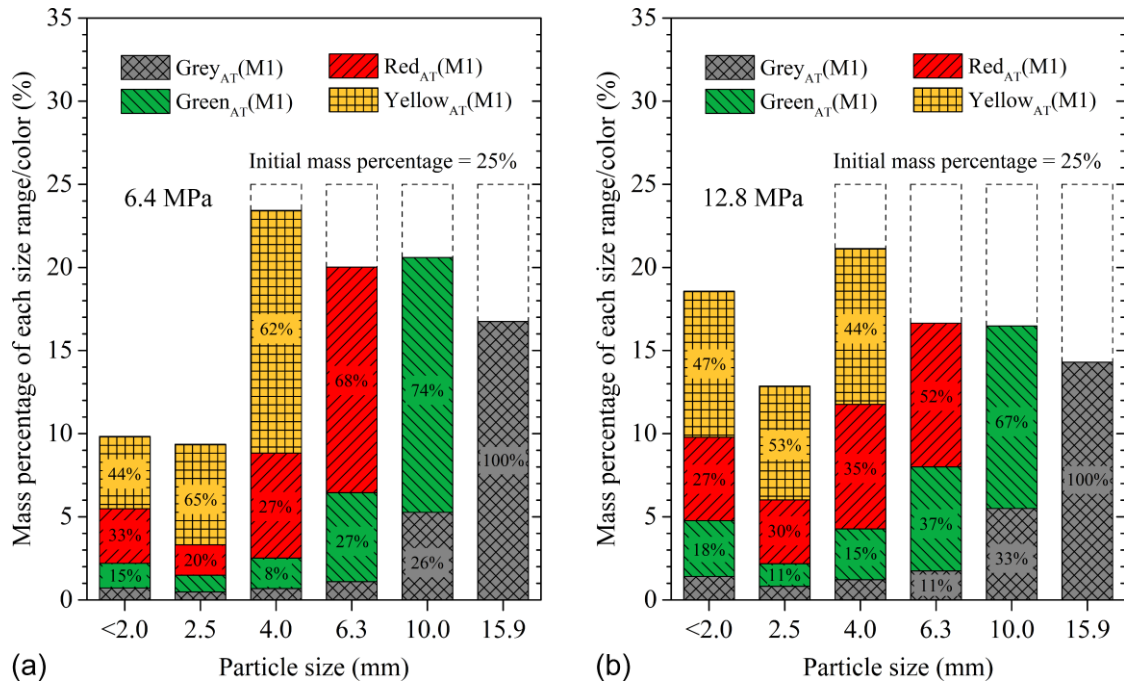


**Fig. 11.** Mass percentage of AT DGPs of different size ranges and colors (a) M1 at 6.4 MPa; (b) M1 at 12.8 MPa.

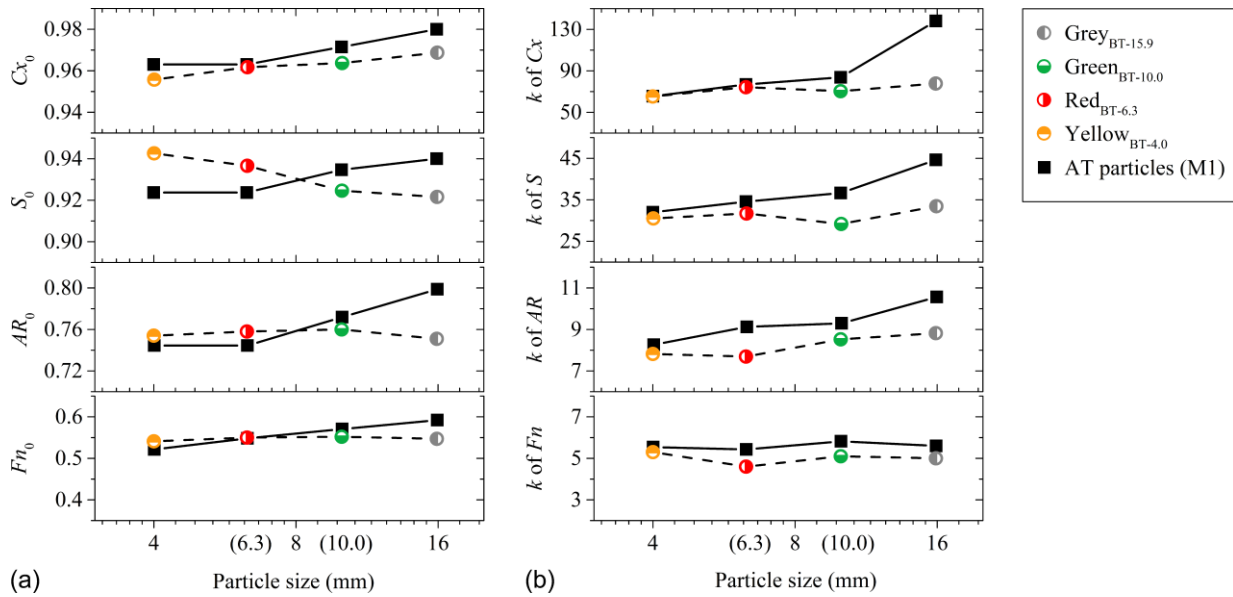


**Fig. 12.** Comparison of particle shape characteristics between AT and BT particles within the same size size ranges (a)  $x_0$ ; (b)  $k$

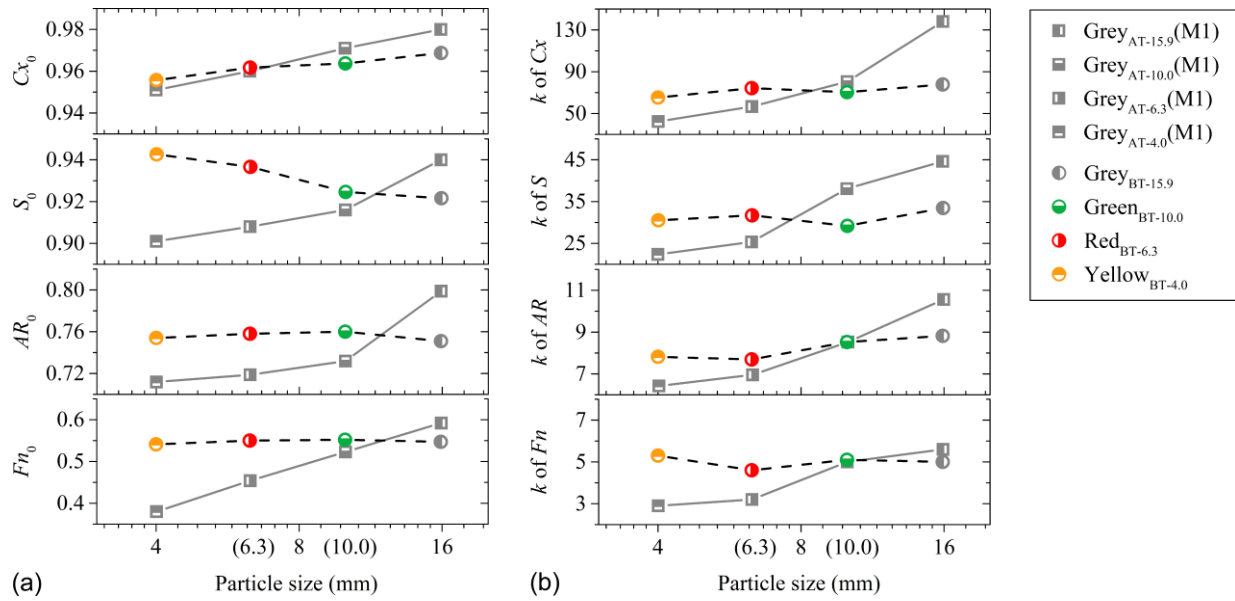


**Fig. 13.** Shape characteristics of AT particles (Grey<sub>AT-15.9</sub>, Grey<sub>AT-10.0</sub>, Grey<sub>AT-6.3</sub>, Grey<sub>AT-4.0</sub>) generated from same-sized parents (Grey<sub>BT-15.9</sub>) compared with those of BT particles (Grey<sub>BT-15.9</sub>, Green<sub>BT-10.0</sub>, Red<sub>BT-6.3</sub>, Yellow<sub>BT-4.0</sub>) (a)  $x_0$ ; (b)  $k$

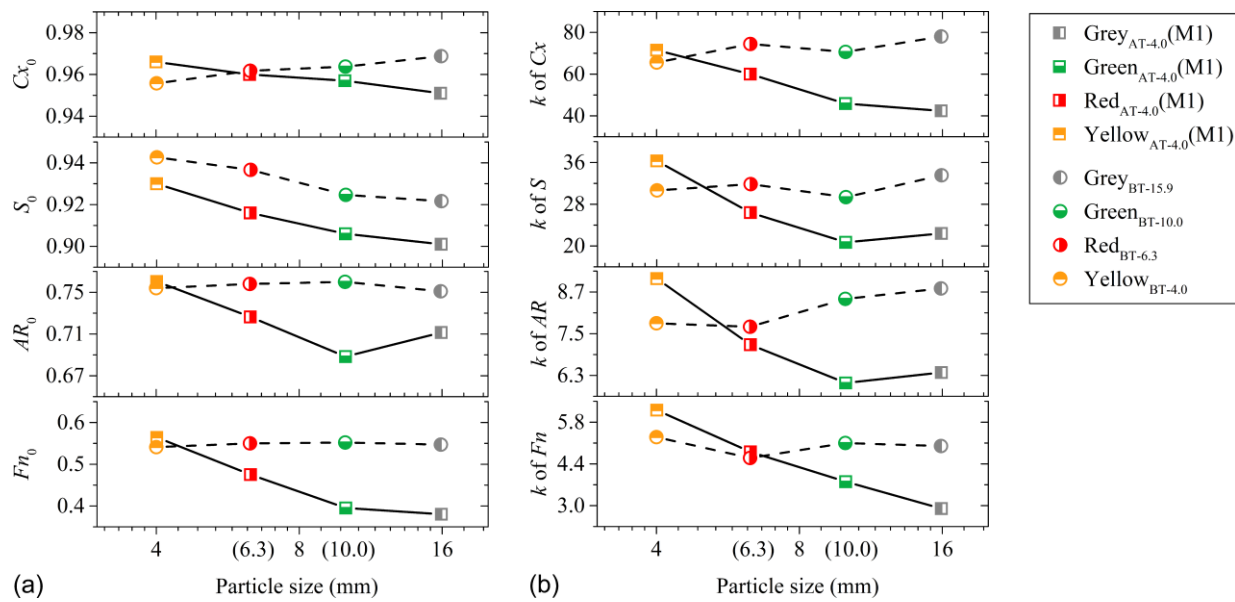


**Fig. 14.** Shape characteristics of same-sized (4.0 mm) children particles (Grey<sub>AT-4.0</sub>, Green<sub>AT-4.0</sub>, Red<sub>AT-4.0</sub>, Yellow<sub>AT-4.0</sub>) from different origins compared with those of their parents (Grey<sub>BT-15.9</sub>, Green<sub>BT-10.0</sub>, Red<sub>BT-6.3</sub>, Yellow<sub>BT-4.0</sub>) (a)  $x_0$ ; (b)  $k$

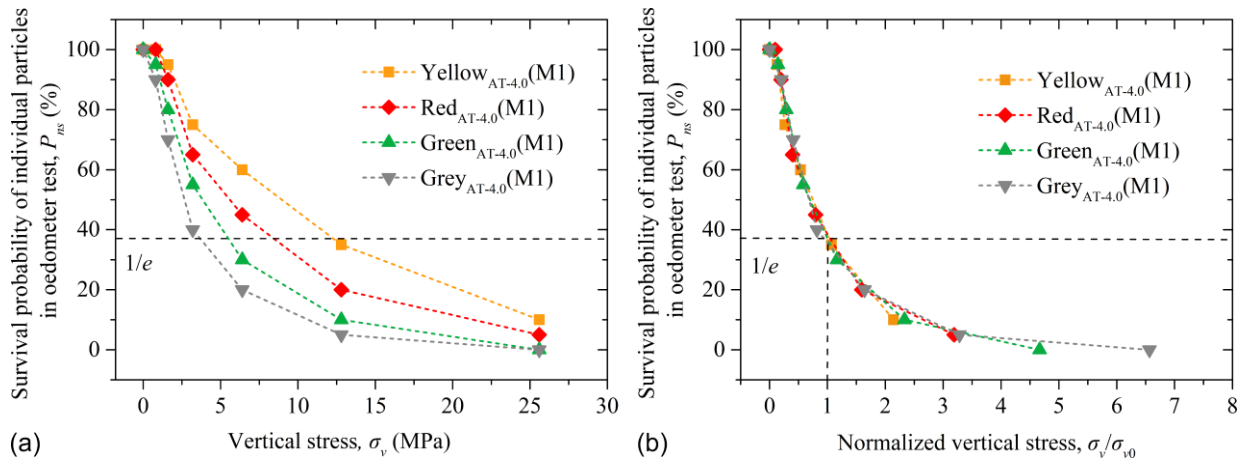


**Fig. 15.** Survival probability of individual 4.0 mm children particles in oedometer test (a) on  $\sigma_v - P_{ns}$  axes;

(b) on  $\sigma_v/\sigma_{v0} - P_{ns}$  ax

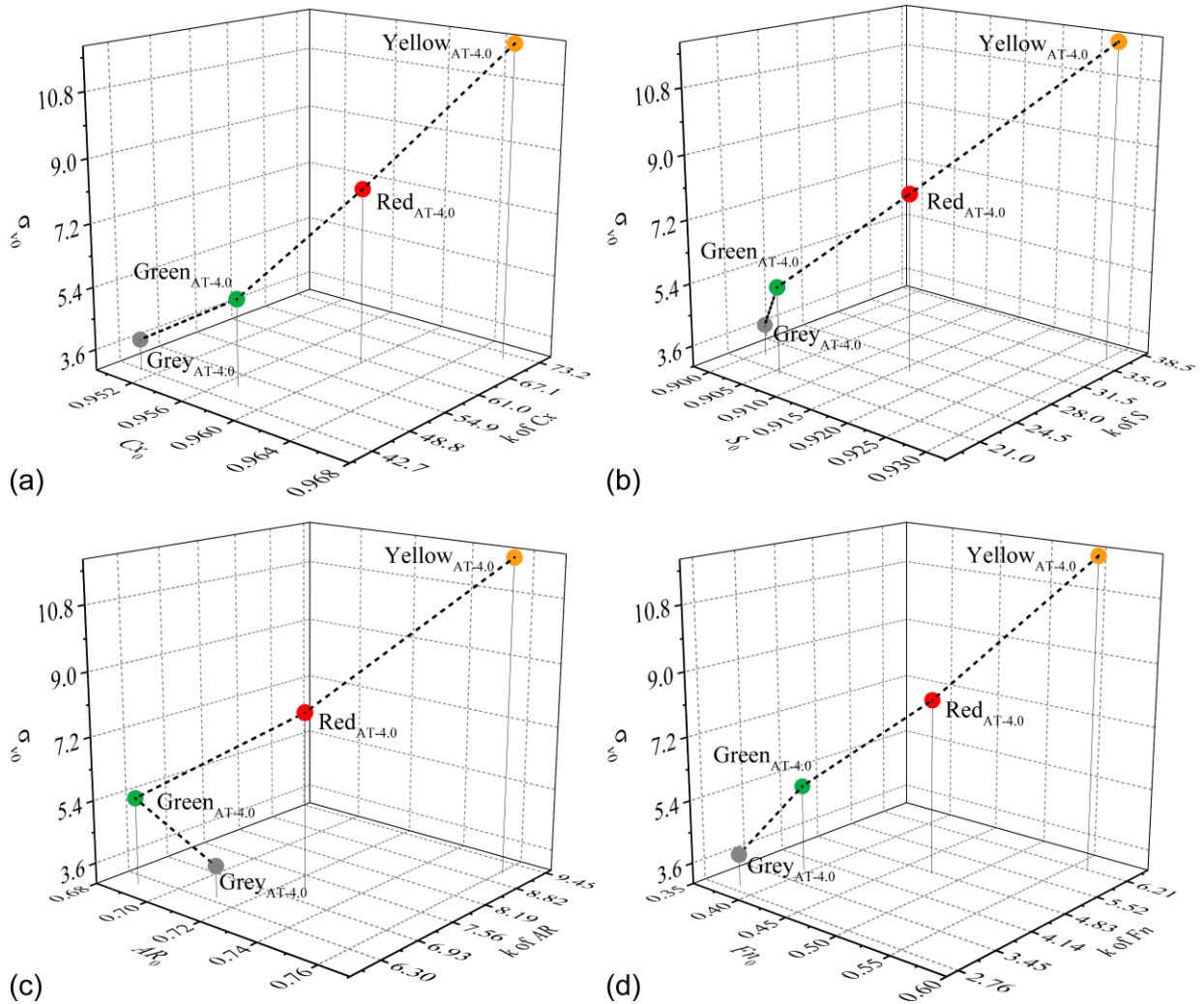


**Fig. 16.** Evolution of the characteristic vertical stress  $\sigma_{v0}$  with changing shape factors (a)  $Cx$ ; (b)  $S$ ; (c)  $AR$ ;  
(d)  $Fn$